

HNPS Advances in Nuclear Physics

Vol 28 (2021)

HNPS2021



Microscopic analysis of structural evolution in the Pt-Hg region

Vaia Prassa, Konstantinos Karakatsanis

doi: [10.12681/hnps.3601](https://doi.org/10.12681/hnps.3601)

Copyright © 2022, Vaia Prassa



This work is licensed under a [Creative Commons Attribution-NonCommercial-NoDerivatives 4.0](https://creativecommons.org/licenses/by-nc-nd/4.0/).

To cite this article:

Prassa, V., & Karakatsanis, K. (2022). Microscopic analysis of structural evolution in the Pt-Hg region. *HNPS Advances in Nuclear Physics*, 28, 79–85. <https://doi.org/10.12681/hnps.3601>

Microscopic analysis of structural evolution in the Pt-Hg region

Vaia Prassa^{1,*}, and K. E. Karakatsanis^{2,3}

¹ Physics Department, Faculty of Science, University of Thessaly, GR-35100 Lamia, Greece,

² Department of Physics, Aristotle University of Thessaloniki, GR-54124 Thessaloniki, Greece,

³ Physics Department, Faculty of Science, University of Zagreb, 10000 Zagreb, Croatia

Abstract The phenomena of shape-phase transitions and shape coexistence in neutron deficient even-even Pt and Hg isotopes are investigated, using a five-dimensional collective Hamiltonian (5DCH) based on covariant density-functional theory. The triaxial deformation energy surfaces in Pt isotopes display a transition from prolate (¹⁸⁸Pt) to triaxial or oblate (¹⁹⁰⁻¹⁹⁸Pt), and to near spherical (¹⁹⁸Pt) shapes. The calculations suggest coexisting configurations in ¹⁹⁰Hg, γ -soft potential energy surfaces in ¹⁹²⁻¹⁹⁸Hg and a more spherical structure in ²⁰⁰Hg. The corresponding 5DCH model calculations confirm the structural evolution in this region but suggest increased collectivity compared to experimental findings.

Keywords Shape transitions; Hg isotopes; Covariant density functionals; Collective states

INTRODUCTION

The phenomena of phase transitions and phase coexistence in even-even nuclei near shell closures have been extensively investigated both theoretically and experimentally (see Refs.[1–6] for reviews). In the region of $Z = 82$ near the neutron midshell $N = 104$ the phenomena of phase coexistence [6] and phase transitions [7] were first observed in studies of hyperfine structure [8]. Later spectroscopic studies [9–18] revealed that the structure of those isotopes was defined by intruder prolate deformed configurations coexisting with less deformed oblate ground states. The low-lying excited states of the intruder band exhibit a parabola shape as a function of neutron number, starting from ¹⁸⁸Hg down to the midshell $N = 104$, with a minimum observed at ¹⁸²Hg and going up to ¹⁸⁰Hg and ¹⁷⁸Hg [19,20]. On the other hand, in the heavier transitional isotopes with $190 < A < 200$, the observed energy levels of the yrast band remain almost constant. Although, the isotopes between the stable ²⁰⁰Hg and the beginning of the midshell in ¹⁹⁰Hg have been investigated by different experiments [21–32], there are still crucial observables that remain to be measured.

Theoretical studies based on the Gogny [33–35], the relativistic mean field (RMF) interactions [36, 37], and the Nilsson-Strutinsky method [38] have generally confirmed these experimental findings. A systematic study of the low-lying states in the lead region has been performed within the number and angular-momentum projected generator coordinate method with axial symmetry, employing the Skyrme energy density functional (EDF) [39]. Excitation energies, electromagnetic transition rates, deformation properties, and ground-state properties relevant to the shape coexistence in Hg isotopes, have been investigated using the interacting boson model (IBM) [40–42]. A recent study within the Elliott and the proxy-SU(3) models [43] suggests that the evolution of shape coexistence in the neutron deficient Hg isotopes is accompanied by a merging of the spin-orbit (SO) - like shell with the open harmonic oscillator (HO) shell [43].

In this contribution we present constrained SCMF calculations for even-even ¹⁹⁰⁻²⁰⁰Hg and ¹⁸⁸⁻¹⁹⁸Pt isotopes within the relativistic Hartree-Bogoliubov [44] method with the density dependent point-coupling (DD-PC1) [45] energy density functional in the particle-hole channel and a separable

* Corresponding author: vprassa@uth.gr

pairing force [46] in the particle-particle channel. The DD-PC1 density functional has been successfully applied to various studies of nuclear structure phenomena related to quantum phase transitions [47–50], shape coexistence [51] and the effect of collective correlations on the ground state and fission properties of superheavy nuclei [52, 53].

A five-dimensional collective Hamiltonian (5DCH) with quadrupole deformations as dynamical collective coordinates [54, 55] is used to calculate the low-energy excitation spectrum and the $B(E2)$ transitions rates. The microscopic self-consistent solutions of deformation-constrained triaxial relativistic Hartree-Bogolyubov (RHB) calculations, the single particle wave functions, occupation probabilities, and quasiparticle energies, are used to calculate the Hamiltonian parameters. The moments of inertia are calculated with the Inglis-Belyaev formula [56, 57] and the mass parameters with the cranking approximation [58]. The collective potential is obtained by subtracting the zero-point energy corrections [58] from the total energy that corresponds to the solution of constrained triaxial SCMF calculations. The resulting collective potential and inertia parameters as functions of the collective coordinates determine the dynamics of the 5DCH. Calculations shown here have been partially presented in [59, 60].

POTENTIAL ENERGY SURFACES

To illustrate the rapid change of equilibrium shapes in Fig. 1 we present the potential energy surfaces of even-even $^{190-200}\text{Hg}$ and $^{188-198}\text{Pt}$ isotopes within the SCMF framework with the DDPC1 functional and a separable pairing force. Starting with the lighter isotope ^{190}Hg the energy surface is γ -soft with two minima within an energy difference of 500 keV, which indicates a case of shape coexistence of the two different configurations. The more pronounced minimum is oblate deformed at $\beta \sim 0.15$ and the second one is prolate at $\beta \sim 0.25$. In ^{192}Hg the energy surface is still rather flat in the γ -direction with the equilibrium configuration on the oblate side at $0.1 < \beta < 0.2$. The prolate minimum diminishes and only the oblate one is seen in $^{194-198}\text{Hg}$. The single oblate minimum becomes less deformed and approaches $\beta = 0$ for ^{200}Hg , which implies a structural change from weakly oblate deformed to nearly spherical states. In Pt isotopes prolate-oblate to near spherical shape transition is predicted. In the isotopes $^{188-196}\text{Pt}$, the prolate or oblate minima are rather extended in the γ -direction, while ^{198}Pt displays a near spherical shape.

The present calculations, based on the relativistic DDPC1 functional, are consistent with other theoretical effort in this region (using the interacting boson model based on the Gogny-D1M EDF [40], the D1 [33] and D1S [34,61] parametrizations of the Gogny-EDF, the Skyrme-SLy4 EDF [35], other Skyrme [39], the relativistic NL3 parametrization [36], and the relativistic PC-PK1 functional [62]).

SPECTROSCOPIC PROPERTIES

The constrained self-consistent solutions of the relativistic Hartree-Bogoliubov (RHB) equations at each point on the energy surface determine the mass parameters the three moments of inertia and the zero-point energy corrections as functions of the deformation parameters β and γ . The diagonalization of the Hamiltonian yields the excitation spectra and collective wave functions that are used in the calculation of various observables, e.g., electromagnetic transition probabilities $B(E2)$ and

electric monopole transition strengths $\rho(E0)$. Physical observables are calculated in the full configuration space and there are no effective charges in the model.

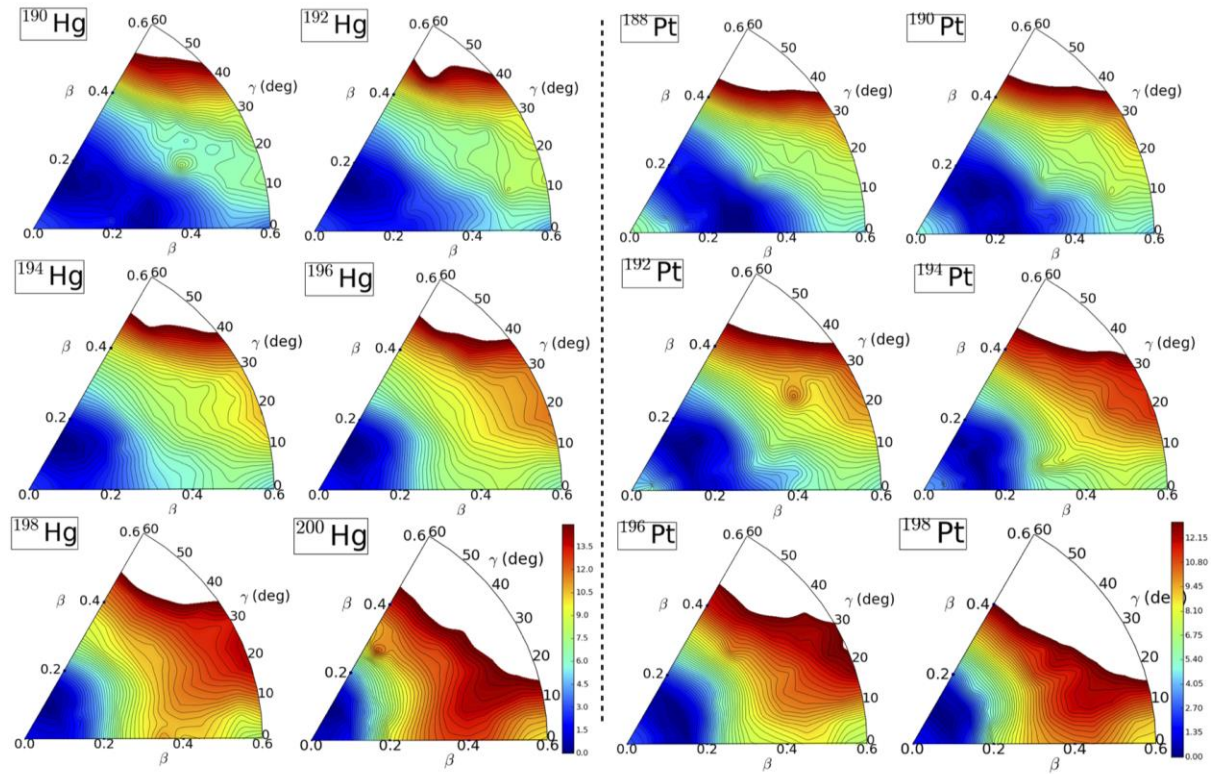


Figure 1. Self-consistent RHB triaxial quadrupole energy surfaces of even-even $^{190-200}\text{Hg}$ and $^{188-198}\text{Pt}$ isotopes in the β - γ plane ($0^\circ < \gamma < 60^\circ$). All energies are normalized with respect to the binding energy of the corresponding ground state.

As an example in Fig. 2 we display the low-lying collective spectrum of ^{196}Hg , in comparison to available data for the excitation energies and reduced electric quadrupole transition probabilities $B(E2)$ in Weisskopf units (W.u.) taken from Refs. [21]. In addition to the yrast ground-state band, in deformed and transitional nuclei excited states are also assigned to (quasi- β) and γ -bands. The comparison with the few existing experimental data shows a rather reasonable agreement of the excitation energy levels in the yrast band for $J^\pi < 6^+$. The theoretical reduced electric-quadrupole transition probabilities $BE(2)$ (in W.u.) are generally larger than the data. Although a reasonable agreement within the experimental errors is observed for the first excited state 2^+_1 , the calculated value for the $B(E2; 4^+_1 \rightarrow 2^+_1)$ overestimates the experimental value considerably. This indicates that there is probably more mixing between the theoretical states than what can be inferred from the data.

In Fig. 3 (left panel) we plot the theoretical values of $R_{4/2}$ as function of the neutron number of even-even $^{190-200}\text{Hg}$ isotopes in comparison to data taken from Ref. [21]. The calculated $R_{4/2}$ ratio starts at 2.32 in ^{190}Hg increases rapidly to 2.64 in ^{192}Hg and then decreases gradually to 2.45 in ^{200}Hg . The experimental values in this region vary slightly around 2.5 as the neutron number increases. The crossing between the 2^+_1 and 4^+_1 normal and intruder states at $N=110$ in Hg is probably the reason for the drop of the ratio $R_{4/2}$ in ^{190}Hg , as reported in Ref. [42]. This effect is less pronounced in the Pt isotopes, Fig.4 (left panel), where the ratio is around 3.3 for $N = 102$ up to $N = 106$ and then decreases gradually with neutron number to approximately 2.5 for $N = 110-118$ (cf. Ref. [62]).

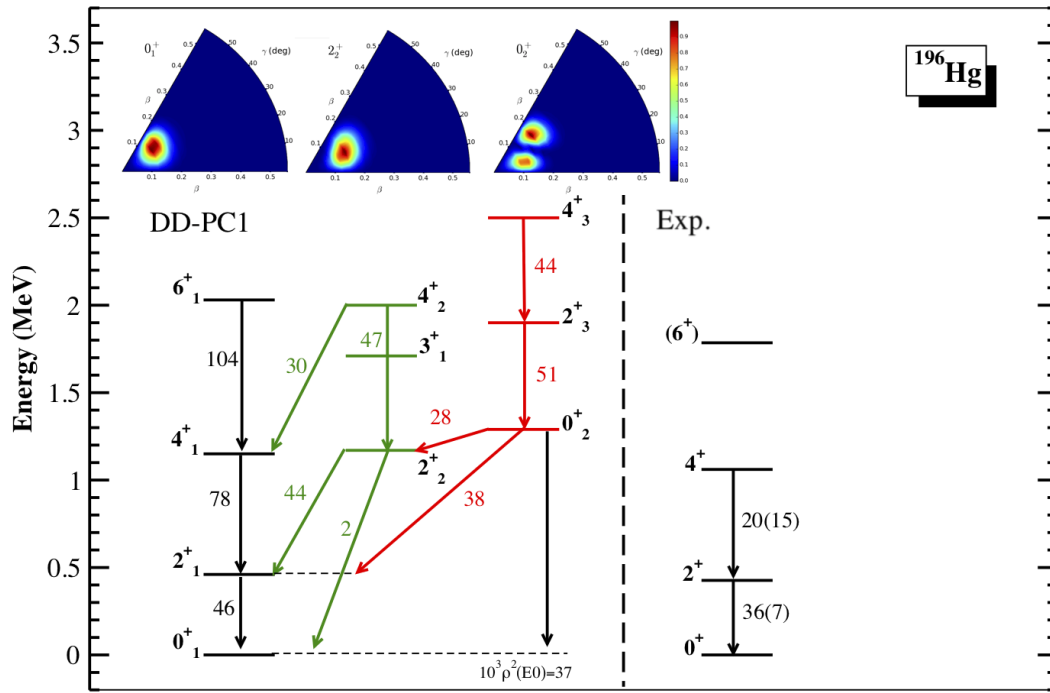


Figure 2. Low-lying level scheme of the even-even ^{196}Hg nucleus. The excitation energies, the $B(E2)$ values (in Weisskopf units) and the $p^2(E0; 0^+_1)$ obtained with the 5DCH based on the DD-PC1 functional are shown. Contour Plots: Probability density distributions in the (β, γ) plane for the three band heads in the yrast band (left), the yrare band (middle), and the excited band built on the state 0^+_2 (right) in the even-even ^{196}Hg nucleus. The experimental data are taken from Ref. [21].

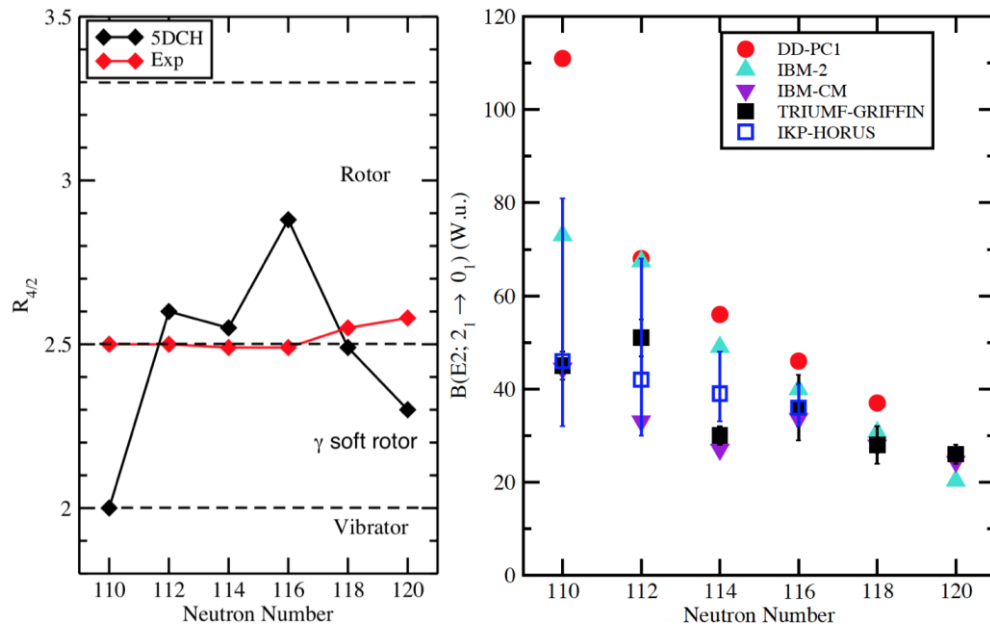


Figure 3. The ratio $R_{4/2}$ of excitation energies of the yrast states 4^+_1 and 2^+_1 (left panel) and the calculated $B(E2; 2^+_1 \rightarrow 0^+_1)$ values (in Weisskopf units) in even-even $^{190-200}\text{Hg}$ isotopes within the 5DCH framework based on the DD-PC1 functional as a function of the neutron number in even-even $^{190-200}\text{Hg}$ isotopes calculated using the 5DCH model based on the DD-PC1 functional. The experimental data are taken from Ref.[21]

In Fig. 3 (right panel) the calculated $B(E2; 2^+_1 \rightarrow 0^+_{11})$ values (in Weisskopf units) in even-even $^{190-200}\text{Hg}$ isotopes within the 5DCH framework based on the DD-PC1 functional are shown. Our calculations reproduce the general decreasing trend with neutron number, however for all isotopes $^{190-198}\text{Hg}$ an increased collectivity in the 2^+_{11} yrast states is observed compared to data. For the isotopes $^{188-198}\text{Pt}$ (Fig. 4 right panel) the accuracy of the calculations compared to the experimental values is of the same quality as the one reached within the PC-PK1 functional.

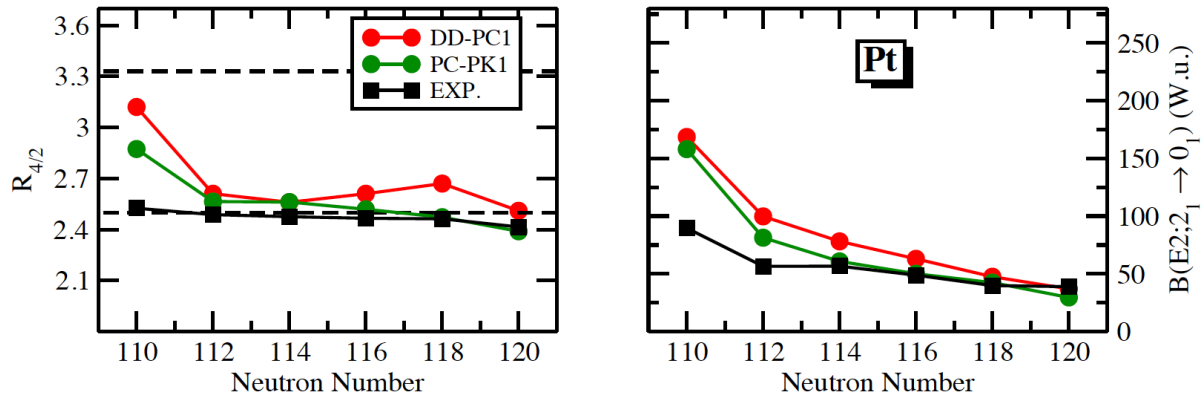


Figure 4. The ratio $R_{4/2}$ of excitation energies of the yrast states 4^+_{11} and 2^+_{11} (left panel) and the calculated $B(E2; 2^+_{11} \rightarrow 0^+_{11})$ values (in Weisskopf units) in even-even $^{188-198}\text{Pt}$ isotopes calculated using the 5DCH model based on the DD-PC1 functional. Results within the PC-PK1 functional (green dots) are taken from Ref. [62]. Experimental data are taken from Ref.[21]

The most noticeable discrepancies between the theoretical calculations and the measured values are consistently in the lighter isotope ^{190}Hg . The potential energy surface of ^{190}Hg exhibits two minima, a dominant oblate configuration and a prolate one at larger deformation that are degenerate in energy with a rather flat path connecting them going through the triaxial region. The inclusion of dynamical correlations yields an oblate deformed but γ -soft 0^+_{11} state and a 0^+_{21} state, within an energy gap of 400keV, that is predominantly on the prolate side but with oblate admixtures. The relatively large overlap between the 0^+_{11} and 0^+_{21} wavefunctions, the large electric monopole transition strength $\rho(E0)$ from the 0^+_{21} to the 0^+_{11} state ($\rho^2(E0; 0^+_{21} \rightarrow 0^+_{11}) \times 10^3 = 150$) and the large $B(E2)$ values of the interband transitions, suggest a strong mixing between the two configurations and support the hypothesis of shape-coexistence at $N = 110$ in Hg.

CONCLUSIONS

Deformation constrained SCMF calculations have been performed with the relativistic Hartree-Bogoliubov method based on the universal energy density functional DD-PC1 and a separable pairing interaction. A quadrupole collective Hamiltonian, with parameters determined by self-consistent constrained triaxial RHB calculations, has been used to calculate the low-energy spectra, $B(E2)$ transitions rates and electric monopole transition strengths $\rho(E0)$ of Hg and Pt isotopes at neutron number $N = 110 - 120$. The calculated excitations energies of the low-lying yrast band in ^{196}Hg reproduce the experimental values, however the $B(E2)$ reduced transition probabilities for the 2^+_{11} and 4^+_{11} yrast states overestimate the data. The two low-lying bands based on the lowest excited vibrational state that appear in the energy spectrum support the hypothesis of increased collectivity in the theoretical calculations compared to data. The evolution with neutron number of the ratio $R_{4/2}$ validate

the above assumptions. In ^{190}Hg , the triaxial SCMF calculations of the energy surface and the results of the quadrupole collective Hamiltonian model suggest shape-coexistence of a dominant oblate configuration and a more prolate deformed intruder state. The triaxial deformation energy surfaces in Pt isotopes display a transition from prolate (^{188}Pt) to triaxial or oblate ($^{190-198}\text{Pt}$), and to near spherical (^{198}Pt) shapes.

Theoretical and experimental efforts in the region of even-even neutron deficient Hg isotopes predict shape transitions from nearly spherical configurations in ^{200}Hg to γ -softness in $^{192-198}\text{Hg}$ and shape coexistence in ^{190}Hg . The results presented in this work verify these findings, demonstrating the potential of the semi-empirical relativistic EDFs including the explicit treatment of collective correlations using a microscopic collective Hamiltonian.

Acknowledgments

V.P.'s research was conducted within the "Call Fellowship for Postdoctoral research" implemented by the University of Thessaly and funded by the Stavros Niarchos Foundation. The work of K.E.K. was financed within the Tenure Track Pilot Programme of the Croatian Science Foundation and the École Polytechnique Fédérale de Lausanne, and the Project No. TTP-2018-07-3554 Exotic Nuclear Structure and Dynamics with funds of the Croatian-Swiss Research Programme. Some of the results presented in this work have been produced using the AUTH Compute Infrastructure and Resources.

References

- [1] K. Heyde, P. Van Isacker, M. Waroquier, J. L. Wood, and R. A. Meyer, *Phys. Rep.* 102, 291 (1983).
- [2] J. L. Wood, K. Heyde, W. Nazarewicz, M. Huyse, and P. van Duppen, *Phys. Rep.* 215, 101 (1992).
- [3] A. N. Andreyev, M. Huyse, P. Van Duppen, et al., *Nature (London)* 405, 430 (2000).
- [4] R. Julin, K. Helariutta, and M. Muikku, *J. Phys. G* 27, R109 (2001).
- [5] T. Grahn, A. Dewald, O. Möller, R. Julin, C.W. Beausang, S. Christen, I. G. Darby, S. Eeckhaudt, P. T. Greenlees, A. Görgen et al., *Nucl. Phys. A* 801, 83 (2008).
- [6] K. Heyde and J. L. Wood, *Rev. Mod. Phys.* 83, 1467 (2011).
- [7] P. Cejnar, J. Jolie, and R. F. Casten, *Rev. Mod. Phys.* 82, 2155 (2010).
- [8] Bonn, J., G. Huber, H.-J. Kluge, L. Kugler, and E.W. Otten, 1972, *Phys. Lett. B* 38, 308 (1972).
- [9] Rud, N., D. Ward, H. R. Andrews, R. L. Graham, and J. S. Geiger, *Phys. Rev. Lett.* 31, 1421 (1973).
- [10] Proetel, D., R. M. Diamond, and F. S. Stephens, *Phys. Lett. B* 48, 102 (1974).
- [11] Hamilton, J. H., et al., *Phys. Rev. Lett.* 35, 562 (1975).
- [12] Cole, J. D., et al., *Phys. Rev. Lett.* 37, 1185 (1976).
- [13] G. D. Dracoulis, *Phys. Scr.* 2000, 54 (2000).
- [14] N. Bree, K. Wrzosek-Lipska, A. Petts, A. Andreyev, B. Bastin, M. Bender, A. Blazhev, B. Bruyneel, P. A. Butler, et al, *Phys. Rev. Lett.* 112, 162701 (2014).
- [15] L. P. Ganev, M. Hackstein, R. D. Page, et al., *Phys. Rev. C* 89, 024307 (2014).
- [16] R. Julin, T. Grahn, J. Pakarinen, and P. Rahkila, *J. Phys. G: Nucl. Part. Phys.* 43, 024004 (2016).
- [17] B. A. Marsh, T. Day Goodacre et al., *Nat. Phys.* 14, 1163 (2018).
- [18] S. Sels, T. Day Goodacre, B. A. Marsh et al., *Phys. Rev. C* 99, 044306 (2019).
- [19] C. Müller-Gatermann et al., *Phys. Rev. C* 99, 054325 (2019).
- [20] J. Elseviers, A. N. Andreyev, et al., *Phys. Rev. C* 84, 034307 (2011).
- [21] B. Olaizola et al., *Phys. Rev. C* 100, 024301 (2019).
- [22] A. Esmaylzadeh, L. M. Gerhard, et al. *Phys. Rev. C* 98, 014313 (2018).
- [23] National Nuclear Data Center (NNDC), Nuclear Levels and Gamma Search.
- [24] M. O. Kortelahti, E. F. Zganjar, J. L. Wood, et al, *Phys. Rev. C* 43, 484 (1991).
- [25] A. Bockisch, K. Bharuth-Ram, A. M. Kleinfeld, and K. P. Lieb, *Z. Phys. A* 289, 231 (1979).
- [26] Th. J. De Boer, E.W. Ten Napel, and J. Block, *Physica* 29, 1013 (1963).
- [27] M. Guttormsen, A. Von Grumbkow, et al, *Nucl. Phys. A* 398, 119 (1983).
- [28] R. Kroth, S.K. Bhattacharjee, C. Günther, M. Guttormsen, K. Hardt, H. Hübel, and A. Kleinrahm, *Phys.*

- Lett.B 97, 197 (1980).
- [29] V. Kölschbach, P. Schöler, K. Hardt, D. Rosendaal, C. Günther, K. Euler, R. Tölle, M. Marten-Tölle, and P. Zeyen, Nucl. Phys. A 439, 189 (1985).
- [30] S. A. Hjorth, I. Y. Lee, J. R. Beene, C. Roulet, D. R. Haenni, N. R. Johnson, F. E. Obenshain, and G. R. Young, Phys. Rev. Lett. 45, 878 (1980).
- [31] R. M. Lieder, H. Beuscher, W. F. Davidson, A. Neskakis, and C. Mayer-Böricke, Nucl. Phys. A 248, 317 (1975).
- [32] R. Kroth, K. Hardt, M. Guttormsen, G. Mikus, J. Recht, W. Vilter, H. Hübel, and C. Günther, Phys. Lett. B 99, 209 (1981).
- [33] M. Girod and P. G. Reinhard, Phys. Lett. B 117, 1 (1982).
- [34] J. P. Delaroche, M. Girod, G. Bastin, I. Deloncle, F. Hannachi, J. Libert, M. G. Porquet, C. Bourgeois, D. Hojman, P. Kilcher et al., Phys. Rev. C 50, 2332 (1994).
- [35] O. Moreno, P. Sarriguren, R. Álvarez-Rodríguez, and E. Moya de Guerra, Phys. Rev. C 73, 054302 (2006).
- [36] T. Nikšić, D. Vretenar, P. Ring, and G. A. Lalazissis, Phys. Rev. C 65, 054320 (2002).
- [37] R. Fossion, Dennis Bonatsos, and G. A. Lalazissis, Phys. Rev. C 73, 044310 (2006).
- [38] R. Bengtsson and W. Nazarewicz, Z. Phys. A 334, 269 (1989).
- [39] J. M. Yao, M. Bender, and P.-H. Heenen, Phys. Rev. C 87, 034322 (2013).
- [40] K. Nomura, R. Rodríguez-Guzmán, and L. M. Robledo, Phys. Rev. C 87, 064313, (2013).
- [41] J. E. García-Ramos and K. Heyde, Phys. Rev. C 89, 014306, (2014).
- [42] J. E. García-Ramos and K. Heyde, EPJ Web of Conferences 178, 05005 (2018).
- [43] A. Martinou, D. Bonatsos, T.J. Mertzimekis, K. Karakatsanis, I.E. Assimakis, S.K. Peroulis, S. Sarantopoulou, and N. Minkov, Eur. Phys. J. A 57, 84 (2021).
- [44] D. Vretenar, A. Afanasjev, G. Lalazissis, and P. Ring, Phys. Rep. 409, 101 (2005).
- [45] T. Nikšić, D. Vretenar, and P. Ring, Phys. Rev. C 78, 034318 (2008).
- [46] Y. Tian, Z. Y. Ma, and P. Ring, Phys. Lett. B 676, 44 (2009).
- [47] K. Nomura, T. Nikšić, and D. Vretenar, Phys. Rev. C 94, 064310 (2016).
- [48] K. Nomura, T. Nikšić, and D. Vretenar, Phys. Rev. C 96, 014304 (2017).
- [49] K. Nomura, D. Vretenar, T. Nikšić, and B.-N. Lu, Phys. Rev. C 89, 024312 (2014).
- [50] V. Prassa, T. Nikšić, and D. Vretenar, Phys. Rev. C 88, 044324 (2013).
- [51] Z. P. Li, T. Nikšić, and D. Vretenar, J. Phys. G: Nucl. Part. Phys. 43, 024005 (2016).
- [52] V. Prassa, T. Nikšić, G. A. Lalazissis, and D. Vretenar, Phys. Rev. C 86, 024317 (2012).
- [53] Z. Shi, A. V. Afanasjev, Z. P. Li, and J. Meng, Phys. Rev. C 99, 064316 (2019).
- [54] Z. P. Li, T. Nikšić, D. Vretenar, P. Ring, and J. Meng, Phys. Rev. C 81, 064321 (2010).
- [55] T. Nikšić, D. Vretenar, and P. Ring, Prog. Part. Nucl. Phys. 66, 519 (2011).
- [56] D. Inglis, Phys. Rev. 103, 1786 (1956).
- [57] S. Beliaev, Nucl. Phys. 24, 322 (1961).
- [58] M. Girod and B. Grammaticos, Nucl. Phys. A 330, 40 (1979).
- [59] V. Prassa and K.E. Karakatsanis, International Journal of Modern Physics E, Vol. 30, No. 7, 2150054 (2021) DOI: 10.1142/S0218301321500543.
- [60] V. Prassa, K. E. Karakatsanis and G. A. Lalazissis (2021) EPJ Web of Conferences 252 02007. DOI: 10.1051/epjconf/202125202007
- [61] http://www-phynu.cea.fr/science_en_ligne/carte_potentiels_microscopiques/carte_potentiel_nucleaire_eng.htm
- [62] X. Q. Yang, L. J. Wang, J. Xiang, X. Y. Wu, and Z. P. Li, Phys. Rev. C 103, 054321 (2021).